

Molecular dynamics simulation on the dissolution and diffusion characteristics of FeCrAl alloy in liquid LBE

Lu Xie^{a,*}, Guang Da Wu^a, Qing Peng^{b,c}, Wen Rui Wang^{a,*}

^a School of Mechanical Engineering, University of Science and Technology Beijing, Beijing 100083, China

^b State Key Laboratory of Nonlinear Mechanics, Institute of Mechanics, Chinese Academy of Sciences, Beijing 100190, China

^c School of Engineering Sciences, University of Chinese Academy of Sciences, Beijing, 100049, China

ARTICLE INFO

Keywords:

FeCrAl alloy
Lead-bismuth eutectic
Dissolution and diffusion
Solid–liquid interface
Molecular dynamics

ABSTRACT

Lead-bismuth eutectic (LBE) corrosion-resistant materials are crucial for the development of future fourth-generation nuclear reactors, and the dissolution and diffusion of material components are important processes in LBE corrosion-resistant materials. FeCrAl alloy is an important structural material for fourth-generation reactors, and it is essential to study its dissolution and diffusion processes in liquid LBE. Molecular dynamics simulations (MD) were used to investigate the mutual diffusion process between the FeCrAl alloy and liquid LBE. The dissolution and diffusion abilities of Fe, Cr, and Al atoms in liquid LBE were evaluated using mean-square displacement (MSD) and diffusion activation energy (DAE). Fe atoms exhibited the highest degree of diffusion, while Al atoms showed the lowest degree of diffusion, resulting in a distinct difference in the elemental distribution at the solid–liquid interface (SLI). There was a significant difference in the depth of penetration of Pb and Bi atoms into the FeCrAl alloy matrix, with Bi atoms penetrating deeper. Furthermore, there is a thermal vibration process during the invasion of Pb and Bi atoms into the FeCrAl alloy matrix, which promotes the invasion process of Pb and Bi atoms. In addition, an increase in temperature exacerbates the diffusion of Fe, Cr, and Al atoms in liquid LBE and the process of Pb and Bi atom invasion into the FeCrAl alloy matrix. Our research may contribute to the design of future nuclear-grade FeCrAl alloy and the development of next-generation reactors.

1. Introduction

The lead–bismuth fast reactor, a kind of reactor cooling with the lead–bismuth alloy, has emerged as the most promising reactor type of the fourth-generation nuclear energy system due to its high safety, miniaturization, and high power density (Alemberti, 2016; Jiang et al., 2022; Luo et al., 2023; Wu et al., 2020). The LBE possesses superior neutronics properties, a low melting point, a high boiling point, excellent heat transfer performance, and low chemical activity. The accelerator driven subcritical (ADS) system is currently considered to be the preferred technical approach to overcome the issues associated with nuclear waste and nuclear safety (Wang et al., 2019). LBE can significantly improve the inherent safety and economy, thus becoming a potential material for the ADS target and reactor coolant (Loewen and Tokuhiko, 2003; Kurata, 2011; Eynde, 2001). Despite many advantages, the high temperature, flow rate and density of LBE can lead to structural corrosion of reactor materials under reactor operating conditions. The corrosion mechanisms mainly include dissolution, oxidation, erosion,

and fretting wear. Liquid metal embrittlement influences the tensile, fatigue, creep, and fracture properties of structural materials in the LBE environment. The structural material of the lead-cooled fast reactor is required to withstand not only the corrosion caused by the coolant but also the temperature and radiation (Gao et al., 2020; Chen et al., 2015).

The LBE corrosion of fast reactors is a vital issue associated with lead-based reactors (Jiang et al., 2022; Luo et al., 2023; Zhang and Li, 2008). There is extensive research on the development of structural materials. It is common sense that the surface oxide layers reduce lead–bismuth corrosion on structural materials. An ideal LBE corrosion-resistant oxide film should be sufficiently dense with a slow growth rate. The FeCrAl alloy demonstrate excellent resistance to LBE corrosion. Two generations of nuclear-grade FeCrAl alloy are currently on the market. The first-generation FeCrAl alloy mainly include four elements: Fe, Cr, Al and trace amounts of Y. The second-generation FeCrAl alloy is developed by adding trace elements (Mo, Nb, Ta, Si, Ti, Zr) on the basis of the first-generation alloy.

FeCrAl alloy have a high resistance to LBE corrosion, and most

* Corresponding authors.

E-mail addresses: xielu@ustb.edu.cn (L. Xie), gmbitwrw@ustb.edu.cn (W.R. Wang).

<https://doi.org/10.1016/j.anucene.2023.109983>

Received 30 March 2023; Received in revised form 22 May 2023; Accepted 8 June 2023

Available online 24 June 2023

0306-4549/© 2023 Elsevier Ltd. All rights reserved.

studies conducted from an experimental perspective have focused only on the oxidative corrosion of materials caused by liquid LBE. The corrosion mechanisms of materials by liquid LBE also involve the penetration of liquid LBE into the inner structure of the material and the dissolution and diffusion of the material (Zhang and Li, 2007; Martinelli et al., 2020; Yeliseyeva et al., 2008; Schroer et al., 2014; Benamati et al., 2002). Several studies have shown that the dissolution and diffusion of materials in liquid LBE is also an important indicator (Yeliseyeva et al., 2008; Benamati et al., 2002). However, due to the small timescale, it is difficult to experimentally study material dissolution and diffusion in liquid LBE. Only a few simulations at low time scales exist. Gao et al. (2016) and Gao et al. (2018) applied the embedded-atom method (EAM) of MD methods to simulate the properties of liquid metal. The calculated density and coefficient of thermal expansion agree well with the experimental results. Maulana et al. (2008) studied steel corrosion in liquid lead-cooled reactors using MD method simulations and found that the higher the temperature was, the deeper the penetration depth of Pb and Bi. Zhou et al. (2004) and Belashchenko (2012) improved the embedded-atom model for Ni, Fe and Pb, Bi, respectively, with better agreement with the experimental physical properties. Arkundato et al. (2010) and Arkundato et al. (2012) studied the corrosion phenomenon of Fe in liquid Pb by MD accompanied by diffusion theory. The interaction of Fe with LBE was also studied numerically by evaluating the diffusion coefficient, radial distribution function (RDF) and MSD curve of Fe. Liu et al. (2018) studied the corrosion process of Fe in liquid Pb by using the MD method and generalized embedded-atom method. Zhou et al. (2021) used MD with embedded-atom model potential to study the behavior of the SLI between body-centered cubic (BCC) Fe (1 0 0) and LBE in an anaerobic environment. Haris et al. (2021) noted that MD simulations are a powerful tool to study corrosion inhibitor corrosion inhibition mechanisms at the molecular level. Despite these efforts, the dissolution and diffusion processes are still elusive at the atomistic scale.

In this work, we aim to study the dissolution and diffusion processes of BCC FeCrAl alloy in liquid LBE by means of MD simulations. MD is a widely used simulation technique for studying atomic-scale systems in a variety of applications (Peng et al., 2018; Qin et al., 2020; Qin et al., 2019; Liu et al., 2019; Sun et al., 2021; Xie et al., 2019; He et al., 2021; Xie et al., 2020; Chen et al., 2019; Qin et al., 2021; Xie et al., 2019) and is thus used to study the dissolution and diffusion processes of FeCrAl alloy in this study. The differences in the penetration of Pb and Bi atoms into FeCrAl alloy and the dependence of the penetration behaviour on temperature are investigated by the RDF, diffusion coefficient and SLI. Our investigation is beneficial for the development of nuclear-level FeCrAl alloy.

2. Methods and computational details

The selection of the potential function is crucial in MD simulations and may directly affect the results of the simulation. The EAM developed by Daw and Baskes (1984) has been used extensively in metallic systems. The total energy E of the metallic system can be expressed as:

$$E = \sum_i F_i(\rho_i) + \frac{1}{2} \sum_i \sum_{i \neq j} \phi_{ij}(R_{ij}) \quad (1)$$

where ϕ_{ij} is the pair energy of atoms i and j at a distance of R_{ij} . F_i is the embedding energy of embedding atom i in a region with electron density ρ_i . The principal electron density ρ_i can be expressed as:

$$\rho_i = \sum_{i(i \neq j)} \rho_i^\alpha(R_{ij}) \quad (2)$$

where $\rho_i^\alpha(R_{ij})$ is the electron density distribution function for atom i .

Our simulations are based on the EAM potential developed by Gao et al. (2018), where the parameters of Zhou et al. (2004) are used for Fe, Al, the parameters of Lin et al. (2008) are used for Cr and Belashchenko

(2012) for Pb and Bi. In order to make the parameters for Fe, Cr, Al and Pb, Bi compatible, we scaled the parameters of Zhou and Lin with a scaling factor μ . The same scaling factor should be used for the same set of parameters, otherwise it would break the intrinsic consistency of the potential parameters. By redefining the electron density ρ_i and potential energy function F_i , which ensures that the total potential energy calculated is the same:

$$F_i'(\eta) = F_i(\eta/\mu) = F_i[(\mu \times \rho_i)/\mu] \quad (3)$$

The choice of individual electron density is arbitrary. Zhou and Lin used the same density standard in their parameters, while Belashchenko used a different density standard. We modified the density function ρ_i^α for Fe, Cr, and Al, while keeping the parameters for Pb and Bi unchanged, to ensure the same density standard for both:

$$\rho_i^\alpha(R) = \mu \times \rho_i^\alpha(R) \cdot F_i'(\eta) = F_i(\eta/\mu) \quad (4)$$

Where, i represents the element Fe, Cr, or Al. The choice of scaling factor μ is crucial. The parameters provided by Zhou and Lin include 17 metallic elements, including the Pb element but not the Bi element. We set the scaling factor $\mu = 0.0097$, which is the same as the value set by Gao et al. (Gao et al., 2018). They used MD simulations and first-principles calculations to complete the diffusion simulation of Fe and Ni in LBE. This method of setting the scaling factor is applicable to matching all metallic elements involved in the Zhou parameters with the Pb and Bi parameters in the Belashchenko parameters. By setting the scaling factor μ , the electron density at $R = 3.00 \text{ \AA}$ for Pb using Zhou's parameters and Belashchenko's parameters were made identical. This result was obtained through X-ray scattering and MD simulations using the EAM potential (Gao et al., 2018). As a result, compatibility was achieved between the parameters of Fe, Cr, Al and those of Pb, Bi. Furthermore, Zhou et al. (2021) and Chen et al. (2023) successfully applied the EAM potential function to the systems of Pb, Bi and bcc-Fe. Further validation of the EAM potential function will be discussed in Section 3.1.

We simulated the dissolution and diffusion of FeCrAl alloy in liquid LBE, and the model is shown in Fig. 1. The LAMMPS software package was used for the MD simulations in this study. The size of the simulation box is $9.17824 \text{ nm} \times 9.17824 \text{ nm} \times 20 \text{ nm}$. To mitigate the effects of anomalous interactions between Pb, Bi and Fe, Cr, Al atoms due to their initial proximity, we introduced an initial gap of 1.5 \AA between liquid LBE and FeCrAl alloy. To resolve the effects of periodic boundary conditions in the z -direction, four layers of fixed atoms were set at the top and bottom of the model. There are 13,971 Pb atoms and 17,075 Bi atoms. There are 43,692 atoms of Fe, 8398 atoms of Cr, and 13,446 atoms of Al. The entire experiment was conducted at a temperature of 693 K. The lattice constant of the FeCrAl alloy was set to $a = 2.8682 \text{ \AA}$, and the crystal structure was BCC. The simulation timestep is 0.001 ps. The initial temperature is 300 K. After 500 ps, the temperature is raised to 693 K and then relaxed for 50 ps with the canonical ensemble (NVT). The simulation is then continued at a constant temperature of 693 K for 4000 ps.

3. Results and discussion

3.1. EAM potential function verification

To validate the accuracy of the EAM potential function, we constructed a liquid LBE model consisting of 16,000 atoms, with the same Pb and Bi atomic ratios as the parameters of the model in Fig. 1. The number of solute atoms (Fe/Cr/Al) was 17. The RDFs of the solute atoms with Pb and Bi atoms were calculated, and they were compared with the first-principles calculations by Gao et al. (2018) and Xu et al. (2017) at different temperatures, as shown in Fig. 2. The positions of the first peaks in the RDFs of the solute atoms with Pb and Bi atoms are almost identical to the first-principles calculation values. The small differences

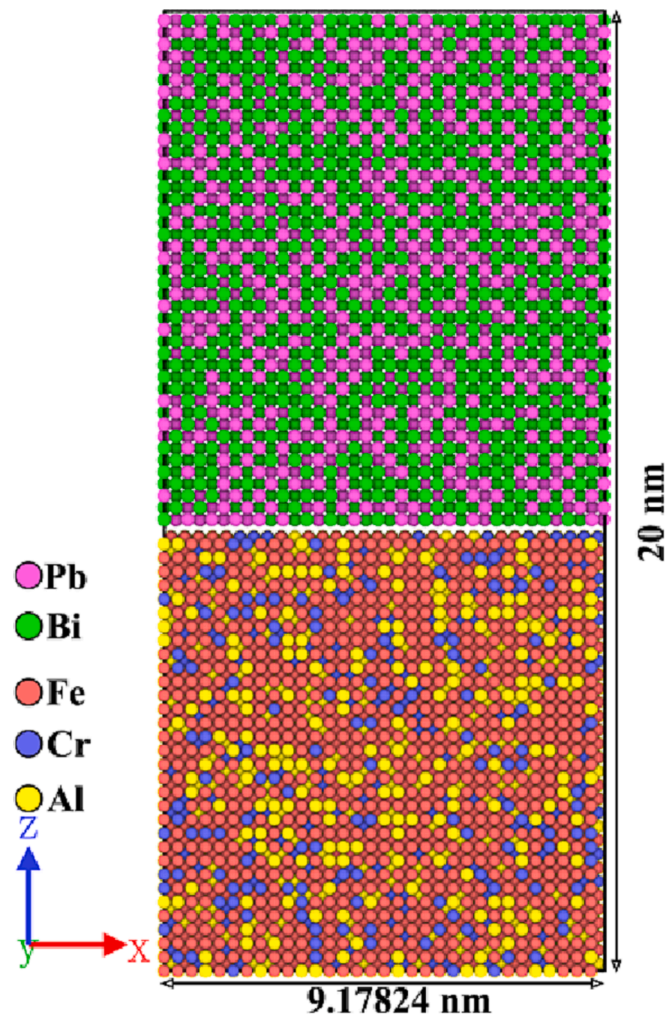


Fig. 1. The initial structure of the FeCrAl-LBE diffusion model (the upper layer is LBE, and the lower layer is FeCrAl alloy).

can be attributed to the increased number of atom types included in the potential function and differences in the calculation methods. The differences in peak intensities are caused by variations in the number of atoms included in the model. Furthermore, we employed the EAM potential function to calculate the melting point of the bcc-FeCrAl alloy, and the obtained range of 1693 K–1820 K is in good agreement with the results reported by McMurray et al. (2017), which were in the range of 1798 K–1813 K.

The dissolution and diffusion processes of solute atoms in liquid LBE are one of the main focuses of this study. To ensure the accuracy of the dissolution and diffusion processes of FeCrAl alloy in liquid LBE, the self-diffusion coefficient (D) of Fe, Cr, and Al atoms in liquid LBE were calculated. D is calculated from the MSD (Qin et al., 2019; Sun et al., 2019), which is a measure of the deviation of a particle from its reference position after it has moved over time (Liu et al., 2018; Zhou et al., 2021). MSD is the most common measure in the spatial range of random motion. It is defined as:

$$MSD = \langle |x(t) - x(0)|^2 \rangle \quad (5)$$

where the $\langle \rangle$ symbol indicates the average of all atoms to be calculated after equilibrium. $|x(t) - x(0)|$ denotes the distance moved by an atom in time interval t . Since atoms diffuse equally in all six directions in the bulk liquid system, self-diffusion coefficient can be derived from the Stokes-Einstein relationship:

$$D = \lim_{t \rightarrow \infty} \frac{1}{6t} MSD \quad (6)$$

D is an important indicator to describe the strength of the diffusion ability of material components in liquid LBE. A larger D indicates faster diffusion. We tested the D s of elemental Fe of FeCrAl alloy in liquid LBE at 673 K, 743 K, 823 K, 873 K, 923 K, and 1023 K, as shown in Table 1. Our calculations are very close to the experimental and simulation results of others, indicating that our simulations are reliable.

In Fig. 3(a), the Arrhenius diagrams for Fe, Cr and Al are shown on the left-Y and below-X, and the D s of Fe, Cr and Al in LBE are shown in relation to temperature on the right-Y and upper-X. The diffusion activation energy (DAE) is calculated according to the Arrhenius equation. The DAEs of Fe, Cr, and Al in the FeCrAl alloy are 0.42 eV, 0.46 eV, and 0.73 eV, respectively. The DAE of pure Fe was calculated to be 0.78 eV from the experimental data reported by Gao et al. (2015). The DAE of pure Fe was calculated to be 0.67 eV from MD data reported by Zhou et al. (2021). Differences between our calculations and those of others may be due to differences in calculation methods and in the types of elements in the system. The MSD of Fe, Cr, and Al atoms were calculated at 693 K (Fig. 3b). The calculated D s for Fe, Cr and Al are $2.65 \times 10^{-11} \text{ m}^2/\text{s}$, $1.87 \times 10^{-11} \text{ m}^2/\text{s}$, $1.95 \times 10^{-12} \text{ m}^2/\text{s}$. The DAE of $\text{Fe} < \text{Cr} < \text{Al}$ lead to a change in the elemental distribution characteristics at the SLI, as shown by the tendency for Fe atoms to be distributed close to the liquid phase and for Al and Cr atoms to be concentrated on the side close to the solid phase, which has also been observed in relevant experimental studies (Jiang et al., 2022; Ren et al., 2022).

Furthermore, we have performed calculations on the mutual-diffusion coefficients between FeCrAl alloy elements and Pb, Bi elements in liquid LBE within the model. The calculation method (Medvedev and Shapiro, 2004) for the mutual-diffusion coefficient M is as follows:

$$M_{ij} = v_i D_i + v_j D_j \quad (7)$$

Where, M_{ij} represents the mutual-diffusion coefficient between different elements i and j , v_i denotes the molar fraction of element i in the system, D_i represents the self-diffusion coefficient of element i , v_j denotes the molar fraction of element j in the system, and D_j represents the self-diffusion coefficient of element j . Our results are consistent with the mutual-diffusion coefficients of pure Fe in liquid lead calculated by Liu et al. (2018) and Robertson (1968), all of which remain within the magnitude of $10^{-9} \text{ m}^2/\text{s}$. In Fig. 4, the mutual-diffusion coefficients between different elements exhibit significant temperature dependence. The mutual-diffusion between Fe and Pb, Bi elements shows the strongest interaction, while the diffusion of Al element is relatively weaker. The above results show that our simulation results are feasible.

3.2. Dissolution and diffusion processes of FeCrAl alloy in liquid LBE

3.2.1. Mutual-diffusion behaviours

Figs. 5 and 6 record the dissolution and diffusion processes of FeCrAl alloy within 4 ns at 693 K. The penetration of liquid LBE into FeCrAl alloy is shown in Fig. 5, and the dissolution and diffusion of Fe, Cr and Al atoms in liquid LBE is shown in Fig. 6. In Fig. 5, Pb and Bi atoms gradually penetrate into the FeCrAl alloy matrix with increasing simulation time. A large number of Bi atoms (green) are observed to aggregate at the SLI, with only a small number of Pb atoms, the penetrate ability of Bi atoms is greater than that of Pb atoms. Furthermore, compared to the dispersed diffusion of Fe and Cr atoms in Fig. 6, Pb and Bi atoms show aggregated diffusion, which is caused by the difference in density between the solid-liquid sides, where the diffusion of atoms in the liquid phase is easier. In Fig. 6(a), the Fe atoms diffuse in the liquid LBE in the greatest amount and depth, followed by the Cr atoms and finally the Al atoms. This phenomenon is related to the difference in the ability of atoms to dissolve and diffuse in liquid LBE. The diffusion

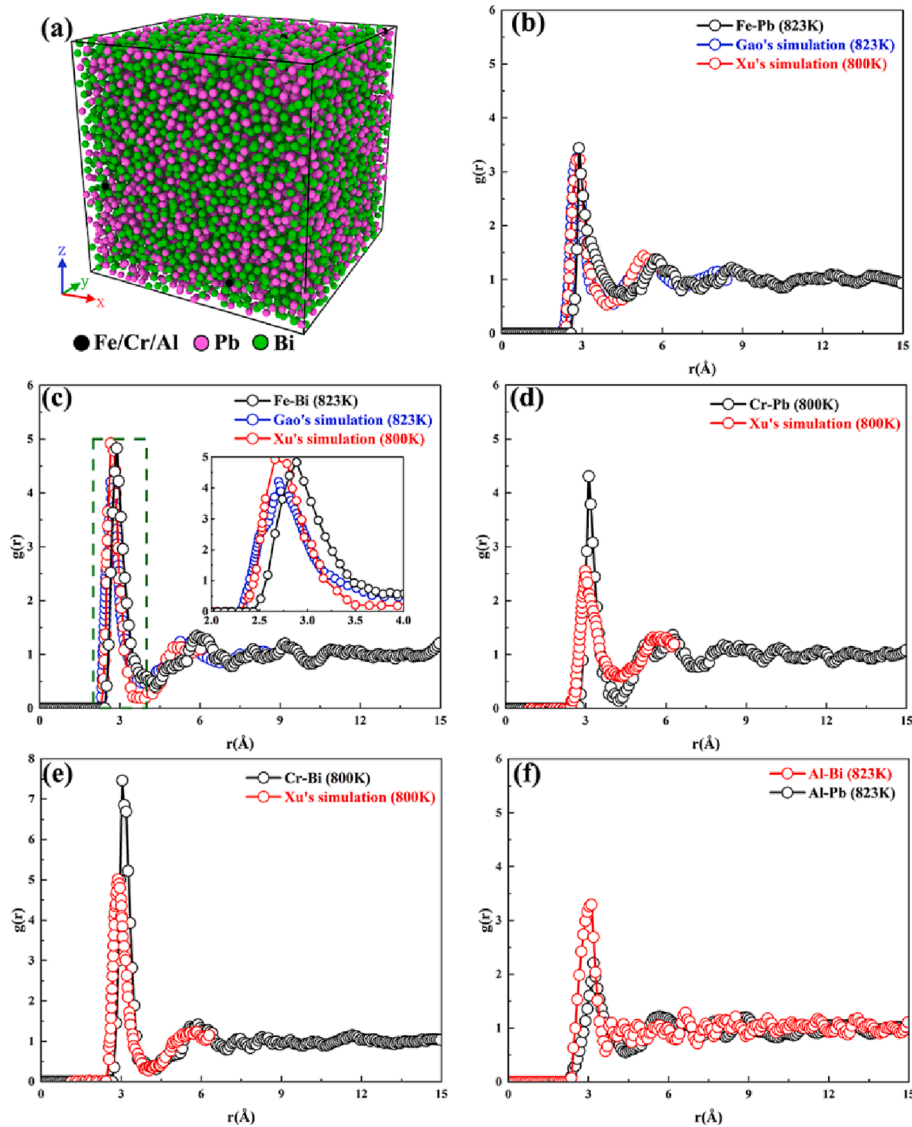


Fig. 2. Diffusion model of solute elements (Fe/Cr/Al) in liquid LBE (a). Radial distribution functions of Fe-Pb (b), Fe-Bi (c), Cr-Pb (d), Cr-Bi (e), Al-Pb and Al-Bi (f).

Table 1
Diffusion coefficient (D) of elements in liquid LBE at various temperatures.

T(K)	Our simulation (m ² /s)		By others (m ² /s)	
	Simulation system		Simulation system	Experiment system
	Fe-Cr-Al in LBE	Fe in LBE	Fe(pure) in LBE	
673	1.68 × 10 ⁻¹¹	2.17 × 10 ⁻¹¹	2.78 × 10 ⁻¹¹ Zhou et al. (2004)	3.50 × 10 ⁻¹¹ Gao et al. (2016)
743	3.13 × 10 ⁻¹¹	4.00 × 10 ⁻¹¹	6.87 × 10 ⁻¹¹ Zhou et al. (2004)	7.60 × 10 ⁻¹⁰ Gao et al. (2016)
823	6.45 × 10 ⁻¹¹	8.00 × 10 ⁻¹¹	7.69 × 10 ⁻¹⁰ Zhou et al. (2004)	7.80 × 10 ⁻¹⁰ Gao et al. (2018)
873	9.05 × 10 ⁻¹¹	1.11 × 10 ⁻¹⁰	8.35 × 10 ⁻¹⁰ Zhou et al. (2004)	1.20 × 10 ⁻⁹ Gao et al. (2018)
923	1.23 × 10 ⁻¹⁰	1.49 × 10 ⁻¹⁰	8.97 × 10 ⁻¹⁰ Zhou et al. (2004)	1.50 × 10 ⁻⁹ Gao et al. (2018)
1023	2.13 × 10 ⁻¹⁰	2.56 × 10 ⁻¹⁰	9.20 × 10 ⁻¹⁰ Zhou et al. (2004)	2.27 × 10 ⁻⁹ Zhang and Li (2008)

activation energies calculated in section 3.1 are Fe < Cr < Al, indicating that Fe atoms need to overcome the smallest energy barrier to diffuse in liquid LBE and Al atoms need to overcome the largest energy barrier,

making it difficult for Al atoms to diffuse into the interior of liquid LBE and preferring to aggregate near the SLI.

Fig. 7 shows the RDF images of Fe, Cr, and Al atoms with Pb and Bi atoms in SLI at 4 ns. The RDF is a measure of the averaged variation in the atomic number density with respect to the distance to the central atom (Qin et al., 2019; Sun et al., 2019; Xie et al., 2018; Song et al., 2013). The results of RDF analysis have the same trend for Fe, Cr, and Al atoms. The RDFs of Fe-Bi and Fe-Pb show a peak near 2.9 Å, and then the peak flattens and oscillates with increasing distance, which indicates a short-range ordered and long-range disordered character, suggesting a liquid state (Fig. 7(b)). In addition, the first peaks of Fe-Bi and Fe-Pb are located at 2.8525 Å and 2.9225 Å, respectively. This result is consistent with the first-principles MD simulations of Xu et al. (2017). They calculated the RDF of Fe dissolved in LBE liquid at 800 K and obtained first peak positions of 2.91 Å and 2.71 Å for Fe-Pb and Fe-Bi, respectively. The discrepancy between our results and first-principles MD simulations may be due to the different temperatures and the increase in element types in the simulations. In Fig. 7, the peaks of Fe, Cr and Al atoms with Bi atoms are much stronger than those with Pb atoms, indicating that the number of Bi atoms in the SLI greatly exceeds the number of Pb atoms. In Fig. 7(d), the peaks of Al atoms are significantly lower compared to the peaks of the Fe and Cr atoms., indicating that Al

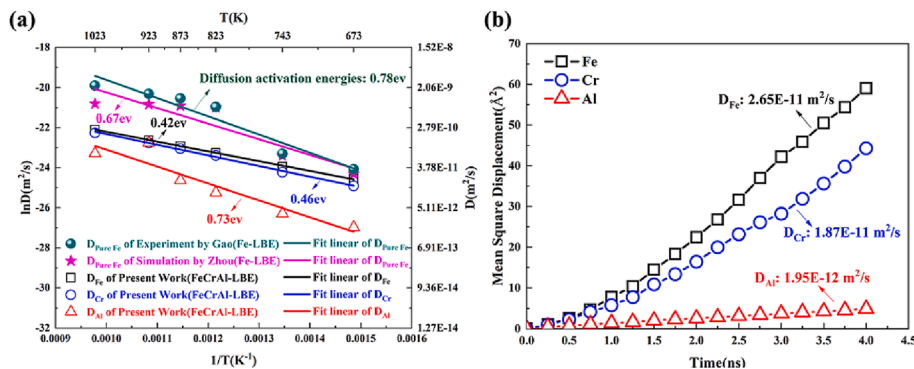


Fig. 3. Arrhenius diagram for diffusion coefficients of Fe, Cr and Al atoms (a). The MSD of Fe, Cr and Al atoms at 693 K (b).

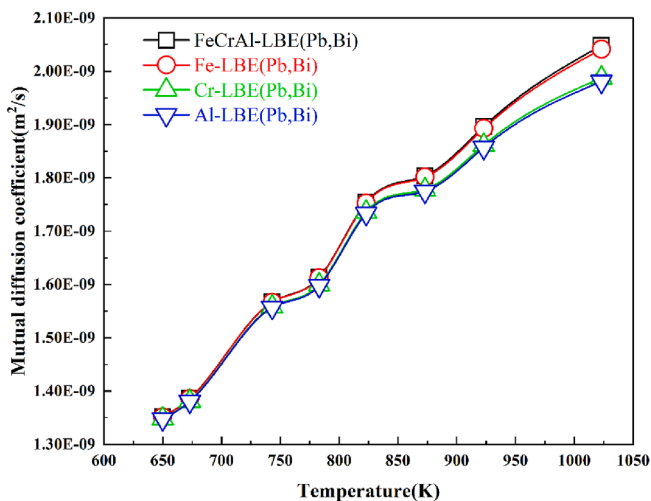


Fig. 4. Temperature dependence of mutual-diffusion coefficients between FeCrAl alloy elements and liquid LBE elements.

atoms are dissolved at the edge of the SLI and basically do not diffuse inside the liquid LBE (Fig. 6c). Furthermore, the peak for Al-Bi occurs at 2.7475 \AA , whereas a very small peak for Al-Pb occurs only near 5.3725 \AA

(Fig. 7d), indicating that the majority of atoms in contact with Al atoms at the SLI are Bi atoms, rather than Pb atoms (Fig. 5). In addition, the first peak of Al-Bi appears at an earlier position than Fe-Bi and Cr-Bi, indicating a stronger interaction between Al and Bi atoms, which may be partly responsible for the lower diffusion of Al atoms into the liquid LBE and causes the repulsive forces generated as the liquid LBE penetrates into the FeCrAl alloy matrix to push the Al atoms to aggregate on the surface of the matrix, even towards the direction away from the SLI (towards the side closer to the solid) (Figs. 6c and 9b).

3.2.2. Solid-liquid interface atom density distribution

We analysed the atom density in the Z direction (Fig. 8). The densities of Bi atoms and Pb atoms far from the SLI are almost the same, and the density of Bi atoms near the initial interface is significantly higher than the density of Pb atoms, indicating that Bi atoms are more active near the SLI. There is a tendency for the density of Fe, Cr and Al atoms to decay near the initial interface, indicating that FeCrAl alloy undergo dissolution and diffusion when in contact with liquid LBE. In contrast, the Al atoms decay more slowly near the initial interface, which is caused by the strong interaction between the Al and Bi atoms pushing the Al atoms closer to the solid side. This typical distribution of elements at the SLI may facilitate the formation of oxide layers of different elements and structures (Jiang et al., 2022; Luo et al., 2023; Wu et al., 2020; Ren et al., 2022).

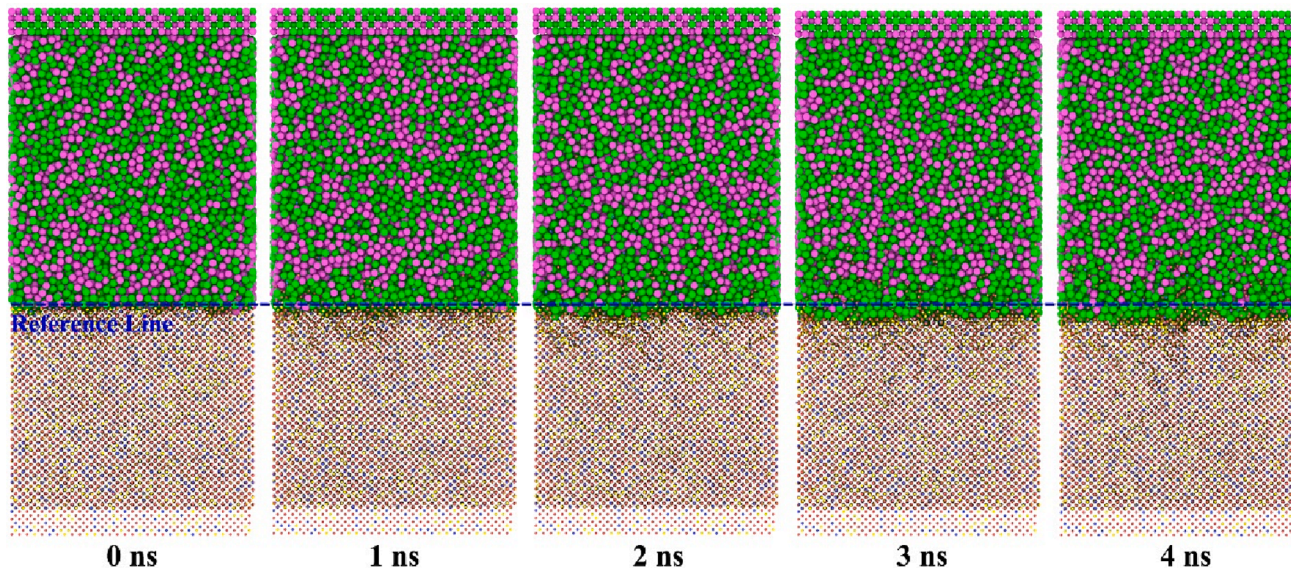


Fig. 5. The mutual-diffusion process of FeCrAl alloy and LBE after system equilibrium at 693 K (The upper layers are Pb and Bi atoms, and the lower layers are Fe, Cr, and Al atoms. The Fe, Cr, and Al atoms are scaled down here for a clear view of Pb and Bi penetration into the FeCrAl alloy matrix.).

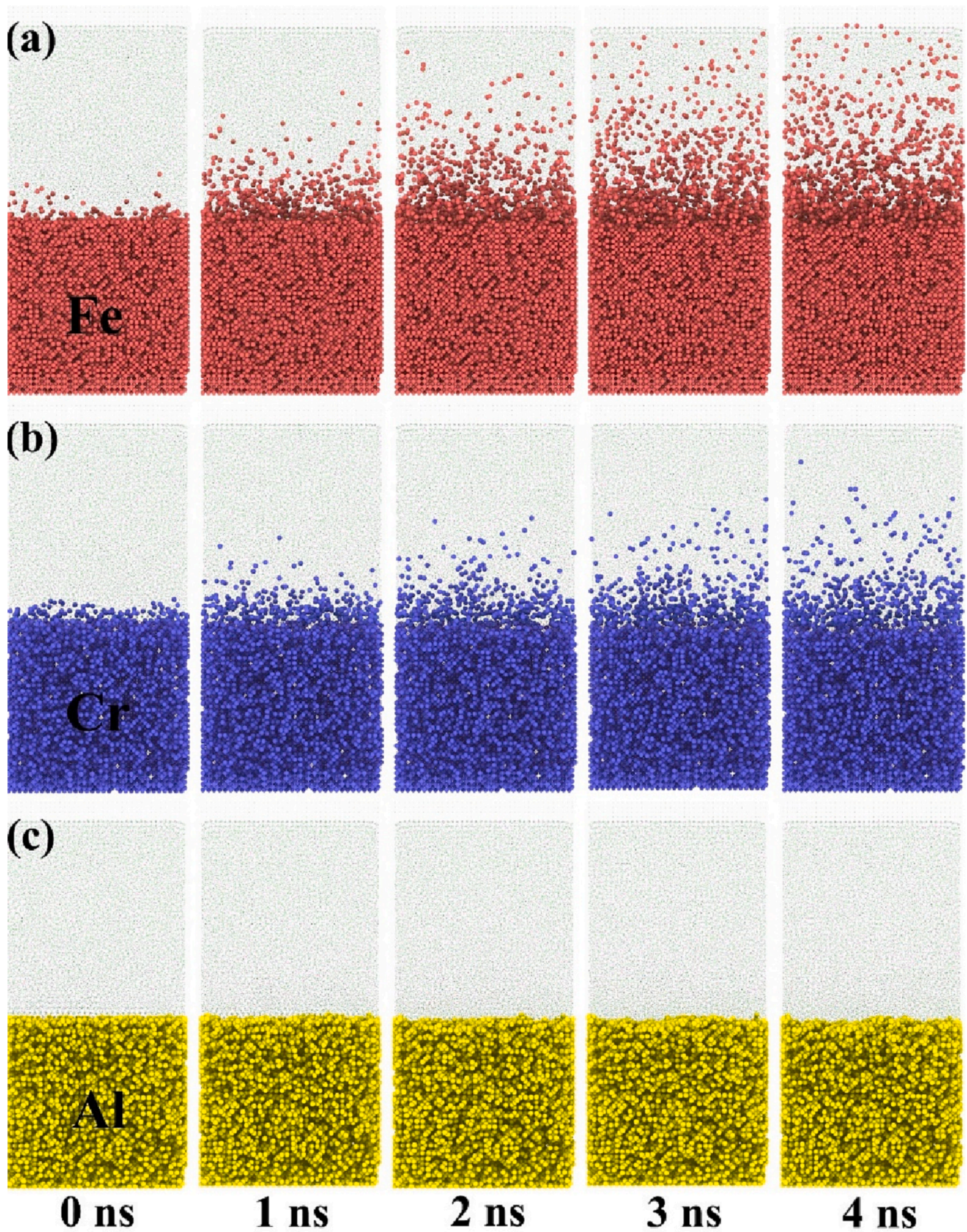


Fig. 6. The mutual-diffusion process of FeCrAl alloy and LBE after system equilibrium at 693 K (To clearly observe the dissolution and diffusion of Fe (a), Cr (b), Al (c) atoms in liquid LBE, the Pb and Bi atoms have been scaled down, and the Fe, Cr, Al atoms are shown separately.).

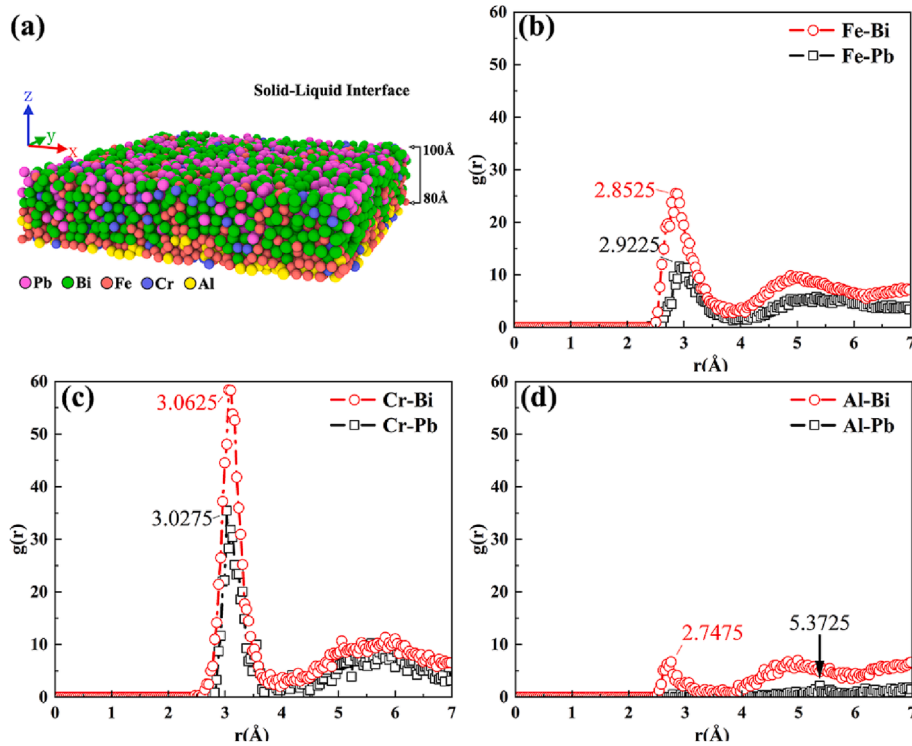


Fig. 7. Atomic morphology of the solid-liquid interface (a). Radial distribution functions ((b) Fe-Bi, Fe-Pb. (c) Cr-Bi, Cr-Pb. (d) Al-Bi, Al-Pb.) of the SLI at 4 ns.

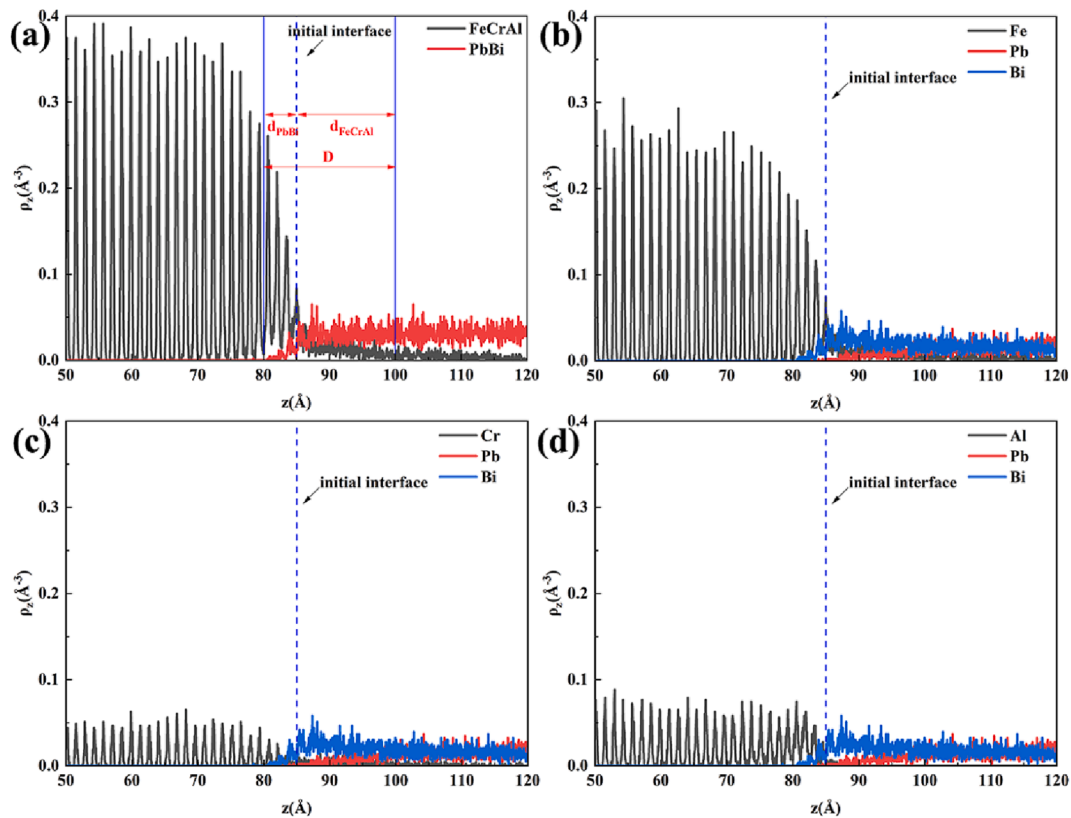


Fig. 8. The distribution of the atom densities of Fe (b), Cr (c), Al (d) and Pb, Bi in the Z direction after equilibrium at 4 ns (d_{PbBi} is the depth of Pb and Bi penetration into the FeCrAl side, and d_{FeCrAl} is the depth of Fe, Cr, Al atom diffusion into the liquid LBE.).

3.2.3. Penetration of FeCrAl alloy by Pb and Bi atoms

We measured the average depth of Pb and Bi atoms penetrating into the matrix of the FeCrAl alloy (Fig. 9a) and the number of Fe, Cr, Al

atoms dissolved into LBE (Fig. 9b). As the simulation time is extended, there is a gradual increase in the depth of penetration of Pb and Bi atoms. Compared to Pb atoms, the penetration depth of Bi atoms is

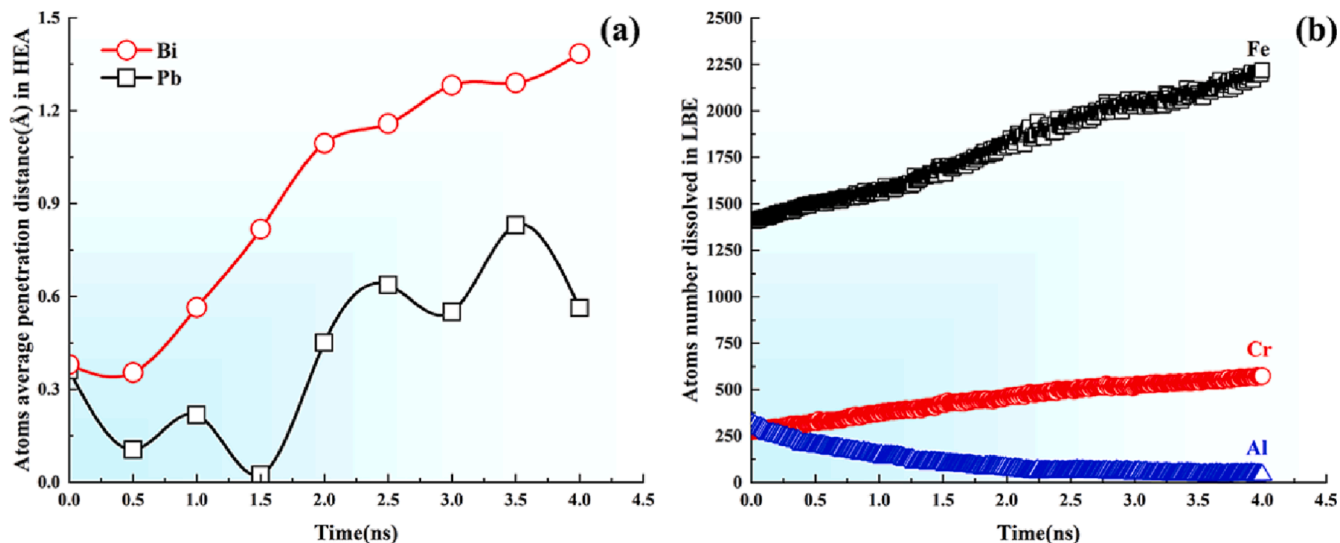


Fig. 9. Average depth of penetration of Pb and Bi atoms into the FeCrAl alloy matrix within 4 ns (a). Number of Fe, Cr and Al atoms diffused into LBE within 4 ns (b).

substantially greater, indicating that the Bi atoms penetrate more easily into the FeCrAl alloy matrix. Furthermore, the average penetration depth of Pb and Bi atoms does not increase monotonically with time (Fig. 9a), indicating that there is a significant thermal vibration of Pb and Bi atoms penetrating into the interior of the FeCrAl alloy matrix (Fig. 10). This process may lead to the re-entry of Pb or Bi atoms penetrating into the FeCrAl alloy matrix into the liquid LBE (Fig. 10). The average depth of penetration of Pb atoms into the FeCrAl alloy matrix at 1.5 ns is close to 0 Å (Fig. 9a), indicating that the Pb atoms penetrating into the matrix are again returned to the liquid phase.

In Fig. 10, this thermal vibrational process of Pb and Bi atoms on the surface or inside the FeCrAl alloy matrix can cause severe lattice distortion, which can lead to atomic bond breakage, causing the matrix atoms to break away from their original positions, facilitating the dissolution of Fe, Cr, and Al atoms into the liquid LBE results in an increased number of vacant spaces for Pb and Bi atoms to penetrate. This also indicates that the corrosion of FeCrAl alloy by liquid LBE does not necessarily leave Pb and Bi atoms inside the matrix but may also cause some vacancy defects. Fig. 9(b) counts the number of atoms dissolved and diffused into the liquid LBE. The highest number of Fe atoms dissolved is related to a higher content of Fe atoms and a relatively small DAE. The number of Al atoms shows a decreasing trend with time, as analysed in sections 3.2.1 and 3.2.2.

The dissolution and diffusion rates of materials in the liquid state generally have a strong temperature dependence. We have analysed the

depth of liquid LBE penetration into FeCrAl alloy varies with temperature (600 K, 650 K, 673 K, 693 K, 743 K, 783 K, 823 K, 873 K, 923 K, 1023 K), and here, the depth of LBE penetration into FeCrAl alloy is expressed in terms of the penetration depth of Pb and Bi atoms. In Fig. 11, the penetration of liquid LBE into the FeCrAl alloy matrix is clearly influenced by temperature, with the depth of penetration increasing with increasing temperature. The temperature effect within the first 2 ns is not very clear because the number of Pb and Bi atoms penetrating into the matrix at the beginning of the simulation is small, and some of the atoms may return to the liquid phase after penetrating into the matrix, leading to a chance in counting the penetration depth. At 750 K, the penetration depth of the LBE is within 1.5 Å at 4 ns. The penetration depth at 750 K–923 K is considerably higher than that at 600 K–750 K, with a substantial increase in penetration depth above approximately 1000 K. At 1023 K and 4 ns, the penetration depth is approximately 7 Å, which corresponds to passing through about five (001) crystal planes. Fig. 12 shows the diffusion results of the system at various temperatures (600 K, 673 K, 783 K, 873 K, 1023 K) simulated at 1 ns. With the rise of temperature, the diffusion of Fe, Cr, and Al atoms with Pb and Bi atoms increases significantly. The high density of Pb and Bi atoms in the form of diffusion contributes to the formation of a similar corrosion profile characteristic of the Al (yellow) atom layer at the solid interface.

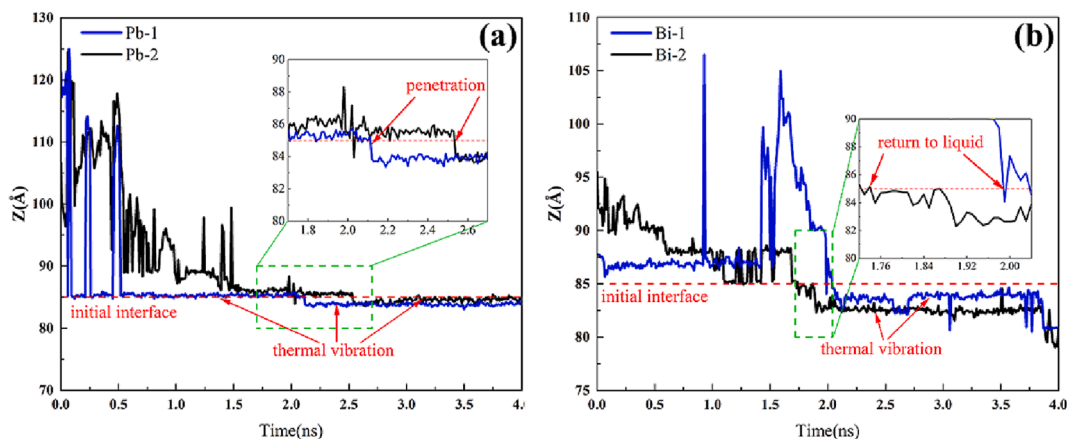


Fig. 10. Trajectories of single Pb (a) atoms and Bi (b) atoms in the z-direction at the SLI (two atoms of each type were taken for analysis).

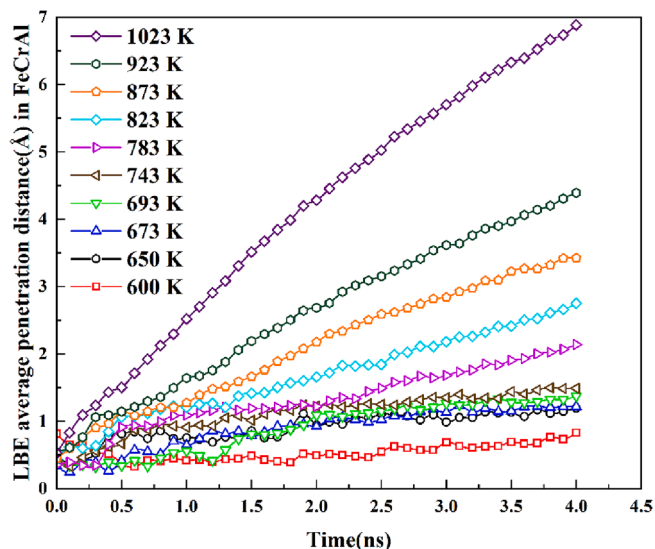


Fig. 11. Temperature dependence of liquid LBE penetration into FeCrAl alloy (the penetration depth of LBE is represented by the penetration depth of Pb and Bi atoms).

4. Conclusions

The dissolution and diffusion processes of nuclear-grade FeCrAl alloy at the atomic level in liquid LBE and the differential penetration ability of Pb and Bi atoms into the FeCrAl alloy matrix were investigated by molecular MD and EAM potentials.

The matrix elements of FeCrAl alloy dissolve and diffuse within a

short time of contact with the liquid LBE, with Fe atoms dissolving and diffusing most readily into the liquid LBE. The diffusion activation energies of Fe, Cr and Al atoms within the liquid LBE are $Fe < Cr < Al$.

The penetration ability of Pb and Bi atoms into the FeCrAl alloy matrix is significantly different, with Bi atoms having a stronger penetration ability than Pb atoms. In addition, there is a significant thermal vibration process during the penetration of Pb and Bi atoms into the matrix, which may lead to vacancy defects in the FeCrAl alloy matrix, further enhancing the corrosion ability of liquid LBE. In addition, the dissolution and diffusion processes of the FeCrAl alloy matrix in liquid LBE and the penetration of Pb and Bi atoms into the matrix are significantly temperature dependent, with an increase in temperature exacerbating the effect of the above processes.

Our atomic-scale insights may provide a boost to the development of nuclear-grade FeCrAl alloy and the application of fourth-generation lead–bismuth reactors.

CRediT authorship contribution statement

Lu Xie: Conceptualization, Formal analysis, Funding acquisition, Investigation, Methodology, Project administration, Resources, Supervision, Writing – original draft, Writing – review & editing. **Guang Da Wu:** Data curation, Formal analysis, Methodology, Validation, Writing – original draft, Writing – review & editing. **Qing Peng:** Funding acquisition, Project administration, Resources, Writing – review & editing. **Wen Rui Wang:** Funding acquisition, Resources, Methodology, Writing – review & editing.

Declaration of Competing Interest

The authors declare that they have no known competing financial

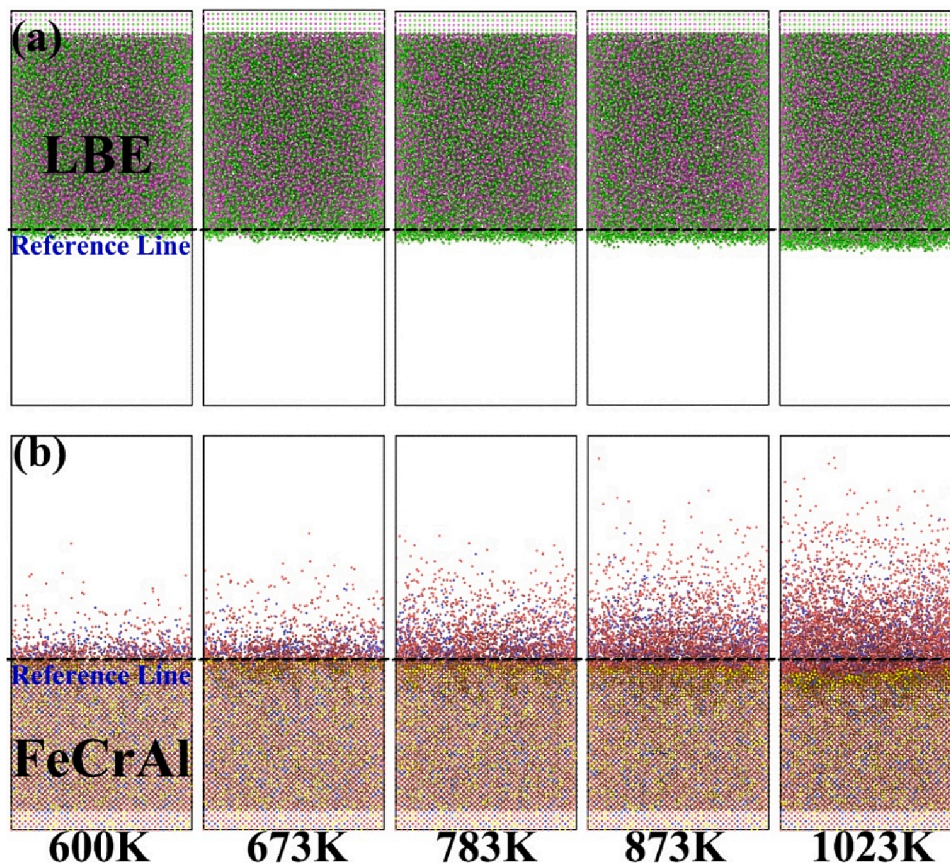


Fig. 12. Diffusion diagram of Fe, Cr, Al (red: Fe atoms, blue: Cr atoms, yellow: Al atoms) atoms (a) and LBE (green: Bi atoms, violet: Pb atoms) (b) at different temperatures at 1 ns. (For interpretation of the references to colour in this figure legend, the reader is referred to the web version of this article.)

interests or personal relationships that could have appeared to influence the work reported in this paper.

Data availability

Data will be made available on request.

Acknowledgement

The authors would like to gratefully acknowledge the financial support from National Key R&D Program of China (Grant No. 2020YFA0405700).

Q. P. would like to acknowledge the support provided by National Natural Science Foundation of China (Grant No. 12272378), and LiYing Program of the Institute of Mechanics, Chinese Academy of Sciences (Grant No. E1Z1011001).

References

- Alemberti, A., 2016. The lead fast reactor: an opportunity for the future? *Engineering* 2 (1), 59–62.
- Arkundato A, Su'Ud Z, Abdullah M. Corrosion Study of Fe in a Stagnant Liquid Pb by Molecular Dynamics Methods. AIP Conference Proceedings 2010.
- Arkundato A, Su'Ud Z, Abdullah M, Widayani, Celino M, Nuclear Physics And Biophysics Research Division PDIT, ENEA CCVA. Numerical study: Iron corrosion-resistance in lead-bismuth eutectic coolant by molecular dynamics method. AIP conference proceedings 2012;1448.
- Belashchenko, D.K., 2012. Computer simulation of the properties of liquid metals: Gallium, lead, and bismuth. *Russ. J. Phys. Chem. A* 86 (5), 779–790.
- Benamati, G., Fazio, C., Piankova, H., Rusanov, A., 2002. Temperature effect on the corrosion mechanism of austenitic and martensitic steels in lead–bismuth. *J. Nucl. Mater.* 301 (1), 23–27.
- Chen, Y., Wang, S., Xie, L., Zhu, P., Li, R., Peng, Q., 2019. Grain size and hydroxyl-coverage dependent tribology of polycrystalline graphene. *Nanotechnology* 30 (38), 385701.
- Chen, J., Wu, Q., Li, J., 2015. Analysis of corrosion oxidation layer of cladding material 316Ti in liquid lead and bismuth. *Atomic Energy Sci. Technol.* 49, 187.
- Chen, L.-M., Xu, S., He, X.-X., Cao, Q.-L., Li, B.-S., 2023. Molecular dynamics study of corrosion behavior of iron with vacancies exposed to lead-bismuth eutectic. *Mater. Corros.* 74 (5), 793–802.
- Daw, M.S., Baskes, M.L., 1984. Embedded-atom method: Derivation and application to impurities, surfaces, and other defects in metals. *Phys. Rev. B* 29 (12), 6443–6453.
- Eynde, G.V.D., 2001. A time-dependent three-dimensional hexagonal-Z transport code. SCK CEN, Mol, Belgium.
- Gao, Y., Takahashi, M., Nomura, M., 2015. Characteristics of iron and nickel diffusion in molten lead-bismuth eutectic. *Mech. Eng. J.* 2, 15.
- Gao, Y., Takahashi, M., Nomura, M., 2015. Experimental study on diffusion of Ni in lead-bismuth eutectic (LBE). *Energy Procedia* 71, 313–319.
- Gao, Y., Raos, G., Cavallotti, C., Takahashi, M., 2016. Molecular dynamics simulation on physical properties of liquid lead, bismuth and lead-bismuth eutectic (LBE). *Procedia Eng.* 157, 214–221.
- Gao, Y., Takahashi, M., Cavallotti, C., Raos, G., 2018. Molecular dynamics simulation of metallic impurity diffusion in liquid lead-bismuth eutectic (LBE). *J. Nucl. Mater.* 501, 253–260.
- Gao, P., Wang, F., Luo, X., 2020. Thermoplasticity of 15–15Ti stainless steel for fast reactor fuel assembly cladding tubes. *Metall. Funct. Mater.* 27, 33.
- Haris, N.I.N., Sobri, S., Yusof, Y.A., Kassim, N.K., 2021. An overview of molecular dynamic simulation for corrosion inhibition of ferrous metals. *Metals-Basel* 11, 46.
- He, C., Pan, G., Xie, L., Peng, Q., 2021. Enhancement of diffusion assisted bonding of the bimetal composite of austenitic/ferrous steels via intrinsic interlayers. *Materials* 14, 2416.
- Jiang, H., Zhao, X., Cao, S., Wang, D., Zhu, Q., Lei, Y., 2022. Effect of Y2O3 addition on the microstructure and liquid LBE cavitation erosion behaviors of Fe-Cr-Al-Ti-C-xY2O3 laser clade coatings. *J. Nucl. Mater.* 572, 154030.
- Kurata, Y., 2011. Corrosion experiments and materials developed for the Japanese HLM systems. *J. Nucl. Mater.* 415 (3), 254–259.
- Lin, Z., Johnson, R.A., Zhigilei, L.V., 2008. Computational study of the generation of crystal defects in a bcc metal target irradiated by short laser pulses. *Phys. Rev. B* 77.
- Liu, S., Xie, L., Peng, Q., Li, R., 2019. Carbon nanotubes enhance the radiation resistance of bcc iron revealed by atomistic study. *Materials* 12, 217.
- Liu, J., Zhao, C.-J., Lu, W.-Q., 2018. Molecular dynamics simulation on the corrosion characteristics of iron in liquid lead. *Ann. Nucl. Energy* 116, 31–41.
- Loewen, E.P., Tokuhiko, A.T., 2003. Status of research and development of the lead-alloy-cooled fast reactor. *J. Nucl. Sci. Technol.* 40 (8), 614–627.
- Luo, W., Huang, Q., Luo, L., Xiao, Z., Wei, J., 2023. Effect of Ce on microstructure evolution of oxide scale for CLAM steel exposed to LBE containing 10–6 wt% oxygen at 500 °C. *J. Nucl. Mater.* 573, 154109.
- Martinelli, L., Ginestar, K., Botton, V., Delisle, C., Balbaud-Célérier, F., 2020. Corrosion of T91 and pure iron in flowing and static Pb-Bi alloy between 450 °C and 540 °C: experiments, modelling and mechanism. *Corros. Sci.* 176, 108897.
- Maulana A, Su'Ud Z, Hermawan KD. Simulation study of steels corrosion phenomenon in liquid leadbismuth cooled reactors using molecular dynamics methods. *Prog. Nucl. Energ.* 2008.
- McMurray, J.W., Hu, R., Ushakov, S.V., Shin, D., Pint, B.A., Terrani, K.A., Navrotsky, A., 2017. Solid-liquid phase equilibria of Fe-Cr-Al alloys and spinels. *J. Nucl. Mater.* 492, 128–133.
- Medvedev, O.O., Shapiro, A.A., 2004. Modeling diffusion coefficients in binary mixtures. *Fluid Phase Equilib.* 225, 13–22.
- Peng, Q., Meng, F., Yang, Y., Lu, C., Deng, H., Wang, L., De, S., Gao, F., 2018. Shockwave generates < 100 > dislocation loops in bcc iron. *Nat. Commun.* 9.
- Qin, Q., He, W., Xie, L., Deng, J., Zhu, X., Peng, Q., 2019. Nonlinear diffusion, bonding, and mechanics of the interface between austenitic steel and iron. *Phys. Chem. Chem. Phys.* 21 (3), 1464–1470.
- Qin, Q., An, H., He, C., Xie, L., Peng, Q., 2019. Anisotropic and temperature dependent mechanical properties of carbon honeycomb. *Nanotechnology* 30 (32), 325704.
- Qin, Q., Sun, T., Wang, H., Brault, P., An, H., Xie, L., Peng, Q., 2020. Adsorption and diffusion of hydrogen in carbon honeycomb. *Nanomaterials-Basel* 10, 344.
- Qin, Q., Liu, X., Wang, H., Sun, T., Chu, F., Xie, L., Brault, P., Peng, Q., 2021. Highly efficient desalination performance of carbon honeycomb based reverse osmosis membranes unveiled by molecular dynamics simulations. *Nanotechnology* 32 (37), 375705.
- Ren, H., Zhang, X., Chen, Y., Zeng, X., Hu, C., Yan, Q., 2022. Synergistic effects of Si and Y on corrosion behavior of cast cladding steels by pre-laying Y powder for nuclear applications in static liquid LBE. *J. Nucl. Mater.* 566, 153781.
- Robertson, W.M., 1968. Diffusion of cobalt and iron in liquid lead measured by grain boundary grooving. *Trans. TMS-AIME* 242, 2139.
- Schroer, C., Wedemeyer, O., Novotny, J., Skrypnik, A., Konys, J., 2014. Selective leaching of nickel and chromium from Type 316 austenitic steel in oxygen-containing lead-bismuth eutectic (LBE). *Corros. Sci.* 84, 113–124.
- Song, C., Li, D., Xu, Y., Pan, B.C., Liu, C.S., Wang, Z., 2013. Ab initio molecular dynamics study of temperature dependent structure properties of liquid lead–bismuth eutectic alloy. *Physica B: Condensed Matter* 429, 6–11.
- Sun, Z., Liu, B., He, C., Xie, L., Peng, Q., 2019. Shift of creep mechanism in nanocrystalline NiAl alloy. *Materials* 12, 2508.
- Sun, Z., Zhang, J., Wang, H., Pan, G., Wang, T., Xie, L., Peng, Q., 2021. Defect, temperature, and strain effects on lattice heat conductivity of egg-tray graphene. *Model Simul. Mater. Sci.* 29 (4), 045003.
- Wang, Z., Yao, C., Qin, Z., Sun, J., Pang, L., Shen, T., Zhu, Y., Cui, M., Wei, K., 2019. Materials for components in accelerator-driven subcritical system. *Chin. J. Eng. Sci.* 21 (1), 39.
- Wu, Z.Y., Zhao, X., Liu, Y., Cai, Y., Li, J.Y., Chen, H., Wan, Q., Yang, D., Tan, J., Liu, H.D., Chen, Y.M., Guo, J.L., Zhang, J., Zhang, G.D., Li, Z.G., Yang, B., 2020. Lead-bismuth eutectic (LBE) corrosion behavior of AlTiN coatings at 550 and 600°C. *J. Nucl. Mater.* 539, 152280.
- Xie, L., An, H., Peng, Q., Qin, Q., Zhang, Y., 2018. Sensitive five-fold local symmetry to kinetic energy of depositing atoms in Cu-Zr thin film growth. *Materials* 11, 2548.
- Xie, L., Sun, T., He, C., An, H., Qin, Q., Peng, Q., 2019. Effect of angle, temperature and vacancy defects on mechanical properties of PSI-graphene. *Crystals* 9, 238.
- Xie, L., An, H., He, C., Qin, Q., Peng, Q., 2019. Mechanical properties of vacancy tuned carbon honeycomb. *Nanomaterials-Basel* 9, 156.
- Xie, L., Sun, T., He, C., Deng, J., Yi, H., Yang, X., Qin, Q., Peng, Q., 2020. Enhancement of toughness of SiC through compositing SiC-Al interpenetrating phase composites. *Nanotechnology* 31 (13), 135706.
- Xu, Y., Zhang, Y., Li, X., Liu, W., Li, D., Liu, C.S., Pan, B.C., Wang, Z., 2017. Effects of iron and chromium on the dynamic properties of oxygen in liquid lead–bismuth eutectic alloy. *Corros. Sci.* 118, 1–11.
- Yeliseyeva, O., Tsisar, V., Benamati, G., 2008. Influence of temperature on the interaction mode of T91 and AISI 316L steels with Pb–Bi melt saturated by oxygen. *Corros. Sci.* 50 (6), 1672–1683.
- Zhang, J., Li, N., 2007. Analysis on liquid metal corrosion–oxidation interactions. *Corros. Sci.* 49 (11), 4154–4184.
- Zhang, J., Li, N., 2008. Review of the studies on fundamental issues in LBE corrosion. *J. Nucl. Mater.* 373 (1-3), 351–377.
- Zhou, T., Gao, X., Ma, Z., Chang, H., Shen, T., Wang, Z., 2021. Atomistic simulation of α -Fe(100)-lead-bismuth eutectic (LBE) solid-liquid interface. *J. Nucl. Mater.* 555, 153107.
- Zhou, X.W., Johnson, R.A., Wadley, H.N.G., 2004. Misfit-energy-increasing dislocations in vapor-deposited CoFe_{0.9}NiFe multilayers. *Phys. Rev. B* 69, 1.